ISSN 1560-8034, 1605-6582 (On-line), SPQEO, 2019. V. 22, N 3. P. 267-276.

Semiconductor physics

Electronic structure, optical and photoelectrical properties of crystalline Si_2Te_3

D.I. Bletskan, V.V. Vakulchak, I.P. Studenyak

Uzhhorod National University, Faculty of Physics, 54, Voloshyna str., 88000 Uzhhorod, Ukraine
E-mail: crystal_lab457@yahoo.com

Abstract. In the framework of the density functional theory (DFT) in the approximation of local density adjusted for the strong correlation (LDA+*U* method), calculated were the band structure, total and partial densities of electronic states, as well as the spatial distribution of the electron density. According to the results of the calculation, Si_2Te_3 is an indirect-gap semiconductor with the calculated band gap E_{gi}^{calc} = 2.05 eV, close to the experimentally measured E_g^{opt} = 2.13 eV. The absorption edge and photoconductivity spectra of Si_2Te_3 crystal within the temperature range 80...293 K have been measured. It has been shown that the dependence of the absorption coefficient on the photon energy is described by the Urbach rule. The parameter σ_0, associated with the constant of electron-phonon interaction, and the energy of effective phonons $\hbar\omega_{ph}$, involved in formation of the absorption edge of crystalline Si_2Te_3, were determined using the temperature dependence of the absorption edge slope. Deviation from the stoichiometric composition in the direction of excess tellurium significantly affects the spectral distribution of the photoconductivity of Si_2Te_3 crystals.

Keywords: silicon sesquitelluride, electronic structure, electron-phonon interaction, absorption edge, photoconductivity.

https://doi.org/10.15407/spqeo22.03.267
PACS 31.10.+z, 71.15.Mb, 71.20.-b, 72.40.+w, 78.20.Ci

Manuscript received 22.05.19; revised version received 18.06.19; accepted for publication 04.09.19; published online 16.09.19.

1. Introduction

Silicon sesquitelluride (Si_2Te_3) is one of binary compounds, which is characterized by the presence of natural defects caused by the peculiarities of their crystal chemistry. Si_2Te_3 crystals contain a large number of stoichiometric cationic vacancies (~10^{27} m^3), with two non-equivalent positions of silicon atoms [1, 2]. The existence of these vacancies and their presence in the crystal do not depend on the method and conditions of its growth. Thus, Si_2Te_3 belongs to a group of semiconductors with positional disordering [3]. It corresponds to the situation where the number of positions of certain types of atoms (in this case silicon) is greater than the number of atoms themselves, and the distribution of atoms by these positions has a partially (or completely) random character.

The layered nature of the structure and the presence of a large number of natural cationic vacancies in Si_2Te_3 crystals favourably contribute to the intercalation of Li^+ and Mg^{2+} ions inside, which opens the possibilities of their practical use as energy storage materials [4]. In addition, silicon sesquitelluride is a thermoelectric material [5]. The increased interest in the study of Si_2Te_3 is also reasoned by the fact that nanoplates [4, 6, 7], nanoribbons [4, 8], nanotapers, and nanowires [8] were recently synthesized by the chemical vapor deposition method (CVD process). These nanostructures are promising materials for use in memory devices [9] and optoelectronics [10].

The nature of chemical bonds, physical and physical-chemical properties of crystals are largely defined by their composition, crystalline and energy structure, as well as the charge of valence electrons distribution. Despite the numerous studies of crystalline structure [1, 2], electrical conductivity, Zeebek coefficient [11-14], reflection and fundamental absorption spectra [15, 16], photoconductivity [17, 18], photoluminescence [7, 18, 19] and vibrational spectra [20] of Si_2Te_3 crystals, the study of their band structure is not

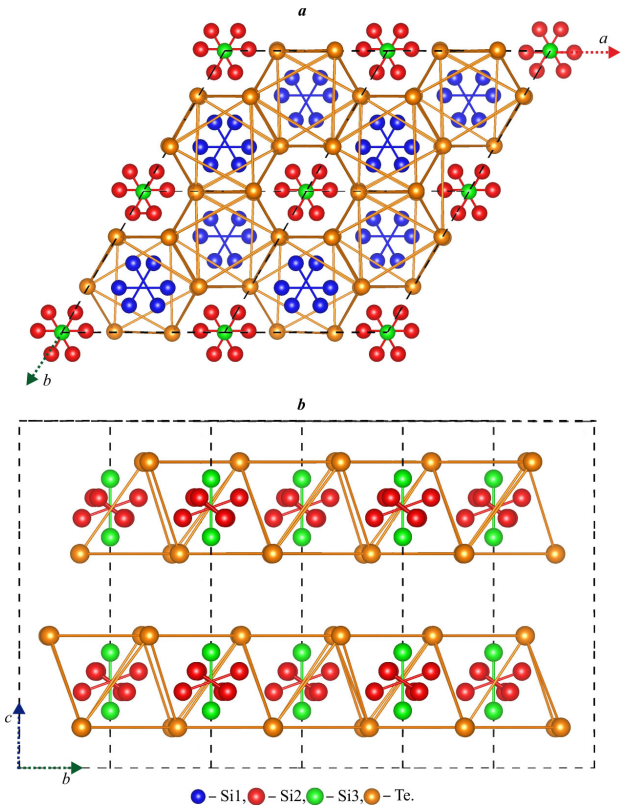

Fig. 1. Si_2Te_3 crystal structure projections on (0001) (*a*) and $(10\bar{1}0)$ (*b*) planes.

numerous [21, 22]. The first results of calculations aimed at the Si_2Te_3 crystal electronic structure performed by the density functional method in the local density approximation (LDA) are given in [21]. In recent paper [22], the influence of the character of Si–Si dimers location in the three-layer package Te–Si–Te on the two-dimensional electronic structure of Si_2Te_3 has been simulated.

This paper presents the results of calculations of electronic structure, total and partial densities of states, distribution of valence charge, as well as the study of the absorption edge and photoconductivity spectra of Si_2Te_3 crystals grown using the static sublimation method.

2. Preparation and crystal structure of Si_2Te_3

The easiest way to obtain the polycrystalline Si_2Te_3 is a direct fusion of elementary components taken in the stoichiometric ratio. As initial components, mono-crystalline silicon and specially purified tellurium were used. The calculated components were loaded into pre-cleaned by chemical-thermal treatment silica ampoules of 160...180-mm length and the diameter of 18...20 mm. Ampoules with the substance were pumped to the pressure of residual gases 133 Pa and sealed. Because of the high pressure of telluric vapors at high temperatures, the synthesis of Si_2Te_3 substance was carried out in two stages. In the first stage, the silica ampoule with the initial mixture was placed in a horizontal tubular resistive furnace and heated to a temperature of 850...900 K at a rate of 0.1 to 0.2 K/h with the next ageing at this temperature for 15...20 hours, whereupon the temperature in the furnace was raised up to 1200 K at a rate of 0.05...0.1 K/s. At this temperature, the melt was held for 24 h to ensure the melt synthesis and homogenization. Then, the programmed temperature reduction was switched on at the set rate 0.2 K/h, and polycrystalline ingot was obtained.

Si_2Te_3 single crystals were obtained by static sublimation method. Crystals were grown in the same ampoules where the synthesis of substance was performed. To reach this aim, without opening the ampoule, the synthesized product was moved by shaking to one end, whereupon the ampoule was placed into a two-zone horizontal tubular electric furnace. Optimal conditions for grown Si_2Te_3 crystal by using the static sublimation method were as follows: temperature of evaporation zone $T_{ev} = 1000$ K; temperature of condensation zone $T_{con} = 900$ K; duration of the growth process 40…50 h. Temperature stabilization in the process of crystal growth was no worse than ±0.5 K. Under these conditions, thin plates were grown in the "cold" zone, the maximum dimensions of which reached 10×10×1 mm. Crystals had natural mirror surfaces (001) with their *c* axis perpendicular to the cleavage face.

Silicon sesquitelluride Si_2Te_3 crystallizes in the trigonal structure, the symmetry of which is described by the space group $P\bar{3}1c$ with the lattice parameters: $a = b = 7.43$ Å, $c = 13.482$ Å [1]. Projections of the crystalline structure on the planes (0001) and $(10\bar{1}0)$ are shown in Figs. 1a and 1b, respectively. The Si_2Te_3 structure is based on hexagonal dense packaging of tellurium atoms in a two-packet form, each containing two layers of tellurium atoms, between which there are silicon atoms in the form of Si_2 dumbbells formations. The layered structure of Si_2Te_3 is generally similar to GaS and is characterized by the statistical distribution of Si atoms on two crystallographically non-equivalent positions in the layers of Te atoms skeleton forming the densest hexagonal packaging. Each Si atom is tetrahedrally coordinated by three Te atoms and one Si atom (Fig. 1). The values of Si–Si (~2.3 Å) distances provide with the opportunity to assert formation of fragments in the form of dumbbells (dimers) Si–Si (Si_2) located, thus, in the centers of slightly distorted [Te_6] octahedra (Fig. 1a).

Unlike GaS, where all Ga–Ga (Ga_2) dimers are oriented parallelly to the trigonal axis, in Si_2Te_3 only 1/4 of Si–Si (Si_2) dimers formed by Si atoms at the position 4e are oriented in parallel to *c* axis (vertical Si–Si dimers). The distances of Si–Si in these "vertical" dimers constitute 2.269 Å and six shortest Si–Te bonds in [Si_2Te_6] octahedra, within which they are located at the distances equal to 2.533 Å. Te–Te distances in triangular faces perpendicular to "vertical" Si_2 dimers is 4.243 Å, the angles Te–Te–Te are equal to 60°. The remaining 3/4 of Si–Si dimers formed by Si atoms in two different positions 12i are located in planes that are approximately

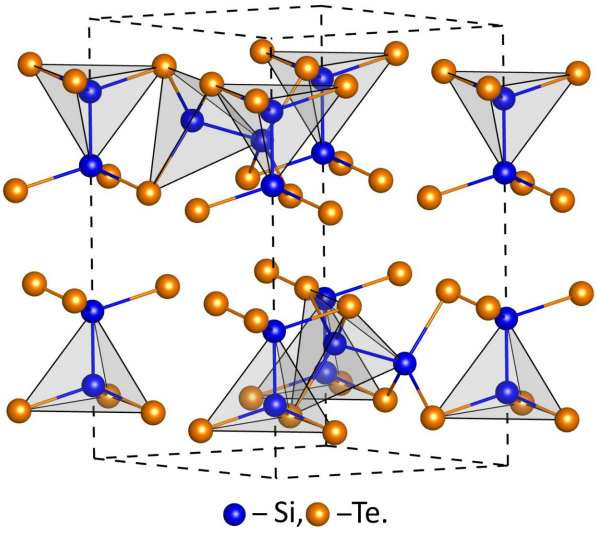

Fig. 2. Elementary cell of Si_2Te_3.

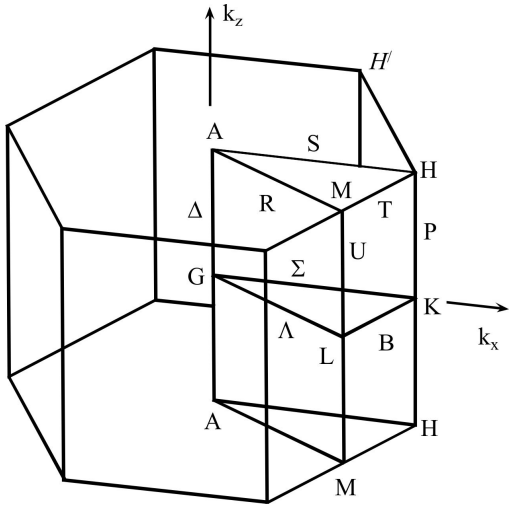

Fig. 3. Brillouin zone of hexagonal Si_2Te_3.

perpendicular to *c* axis with planes (with an angle of inclination equal to approximately 18°) and are oriented by three different ways in such a manner that six Si atoms on average form a six-member cycle. The lengths of Si–Te bonds in containing these "horizontal" Si–Si dimers in weakly distorted [Si_2Te_6] octahedra constitute 2.451 to 2.662 Å. The distances Te–Te in triangular faces perpendicular to the "horizontal" Si_2 dimers constitute 4.36...4.37 Å, and the angles Te–Te–Te are ~60°. The shortest Te–Te interlayer distance is 4.016 Å.

Thus, the most important feature of Si_2Te_3 crystalline structure is the statistical placement of 8 silicon atoms in two positions 12i and one – 4e. These positions are filled with a deficit of 71 percent, because instead of 28 silicon atoms, only 8 are placed in them. In the first position 12i 4 atoms are placed, in the second 12i only 2 atoms and finally in the position 4e also 2 atoms are located. Therefore, both 12i positions are occupied by 1/3 or 1/6, respectively, and position 4e is filled by 50%. As a result, Si_2 dimers inside Si_2Te_3 structure are separated into the "vertical" and "horizontal" ones in the ratio 1:3. The elementary cell taking into account this filling of the Si and Te atoms is shown in Fig. 2.

3. Results and discussion

3.1. Electronic structure and density of states

The electronic structure of Si_2Te_3 crystal was calculated within the framework of density functional theory in LDA and LDA+*U* approximations [23] by using the software package SIESTA [24]. The values of the parameters of direct Coulomb and exchange interactions constituted $U = 7$ eV and $J = 0.7$ eV. The band structure and state density of Si_2Te_3 calculated by LDA+*U* method without taking into account the spin-orbital interaction at all points of high symmetry and along all symmetrical directions in irreducible parts of the Brillouin zone (Fig. 3) are shown in Figs. 4 and 5, respectively.

The last filled state is taken for zero energy. The Si_2Te_3 crystal valence complex consists of 52 dispersion branches grouped into three bundles of bands in the energy intervals –12.88…–10.81, –9.26…–5.63 and –5.02…0 eV separated by forbidden gaps. The total width of the occupied bands is 12.88 eV. The top of the valence band is located in the center of the Brillouin zone, and the bottom of the conductivity band is localized at the point K. Thus, silicon sesquitelluride is the indirect-gap semiconductor with the calculated energy gap $E_{gi} = 2.05$ eV.

Analysis of partial contributions to the total density of states $N(E)$ (Fig. 5) allows identifying the genetic origin of different subzones of the valence band and the conductivity band of Si_2Te_3. The relationships between the intensities of maxima in partial densities of states for various types of symmetry are different. In the depth of the valence band of this compound in the total density of electronic states $N(E)$, the contribution of 5*s* tellurium state dominates, whereas in the upper part of the valence band the contribution of 5*p*-states of Te atoms is dominating. The lowest valence subband located within the energy range from –12.88 to –10.81 eV is mainly formed by 5*s*-states of tellurium. Despite the prevailing nature of Te 5*s*-states, the effects of hybridization of silicon and tellurium atoms states are significant for this subband, leading to the appearance of silicon atoms 3*s*-states contributions that are mostly localized at the bottom of this subband, and Si *s*-, *p*-, *d*-states – at its top.

The middle part of the valence bands in the energy range from –9.26 to –5.63 eV can be separated into four subgroups of relatively isolated subbands, each containing two dispersion branches. The two lower subgroups of four valence bands (–9.26…–5.84 eV) are formed by the hybridized Si 3*s*-, 3*p*- – Te 5*s*-states. The next two upper subgroups have a mixed character with involving 5*s*- and 5*p*-states of Te and 3*s*- and 3*p*-states of Si.

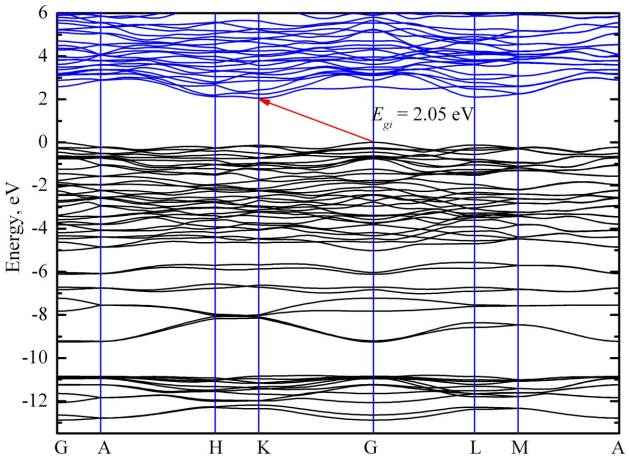

Fig. 4. The electronic structure of Si_2Te_3 calculated in LDA+*U* approximation.

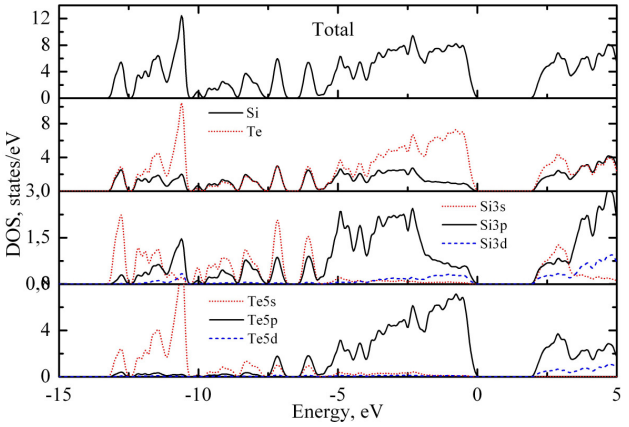

Fig. 5. Full and local partial densities of electronic states of Si_2Te_3 crystal, calculated in the approximation of LDA+*U*.

The most complicated is the upper subband of the occupied states (–5.02...0 eV) consisting of 32 dispersion branches. The very top of this subband, located directly near the top of the valence band (–1.60…0 eV), is mainly formed by 5*p*-states of tellurium with a slight admixture of 3*p*-, 3*d*-states of silicon. The lower part of this subband (–5.02…–1.60 eV) is formed by the hybridized 5*p*-states of tellurium and 3*p*-states of silicon.

The electronic low-energy structure of unfilled electronic states in silicon sesquitelluride is mainly formed by kneading free Te *p*-, *d*- and Si *s*-, *p*-, *d*-states, with predominant contribution of *p*-states inherent to both atoms. Thus, the analysis of full and partial densities of states indicates significant hybridization of *s*- and *p*-states of Si and Te atoms, which evidences for strongly covalent nature of chemical bond Si–Te in $[Si_2Te_6]$ coordination octahedron (structural unit of Si_2Te_3), and the main role in the optical interband transitions should be performed by the transfer of charge between Te 5*p* occupied states and Te *p* + Si *s*, *p* free states in the conductivity band.

3.2. Electronic density distribution

To analyze the chemical bond in crystals, it is convenient to use the spatial distribution of charge (electronic) density $\rho(\boldsymbol{r})$. As an example, Fig. 6 shows electron density distribution maps in four different planes: (a) the plane passing along the links lines Te–Si–Te in $[SiTe_3Si]$ tetrahedron (Fig. 2); (b) and (c) in the plane perpendicular to the four-layer packets Te–Si–Si–Te, passing through the "horizontal" (b) and "vertical" (c) Si_2 dimers; (d) in the plane of the tellurium monolayer.

The shape of contour maps of electronic density clearly indicates that in its composition the contributions of tellurium atoms occupy a noticeably greater part of space than those of silicon atoms. The general contours $\rho(\boldsymbol{r})$ covering silicon and tellurium atoms in $[SiTe_3Si]$ tetrahedra indicate the existence of a covalent component of the chemical bond, formation of which is the responsibility for Si 3*s*-, 3*p*- and Te 5*s*-, 5*p*-states hybridization. Polarization of the charge density in the direction Si→Te indicates the presence of an ion component in addition to the covalent one. Thus, the nature of the electron density distribution indicates the mixed ion-covalent bond type in four-layer packages Te–Si–Te. A characteristic feature of chemical binding in Si_2Te_3 is the presence of common contours $\rho(\boldsymbol{r})$ between three tellurium atoms in the tellurium monolayer (Fig. 6d) belonging to a separate $[Si_2Te_6]$ octahedron, which is not typical for other layered crystals crystallizing in CdI_2 structure, for example $SnSe_2$ [25].

Found in [14] strong anisotropy of electrical properties of the Si_2Te_3 layered crystals becomes clear from the density distribution map of valence electrons carried out in a plane that intersects two four-layer packages, as it is shown in Fig. 6c. The electronic density within the four-layer packets, reflecting the chemical bond of silicon atoms with the nearest neighbors (tellurium atoms) in $[Si_2Te_6]$ octahedral, is much higher than at their boundaries. There are no common level $\rho(\boldsymbol{r})$ lines for adjacent tellurium atoms belonging to two different adjacent four-layer packets, indicating a weak overlap of their wave functions. This spatial anisotropy of electron density and energy distribution of electron 5*p*-states of tellurium is the cause of quasi-two-dimensional nature of silicon sesquitelluride.

3.3. Spectra of the fundamental absorption edge of Si_2Te_3 crystal

Spectral dependences of the absorption coefficient of crystalline Si_2Te_3, measured at various temperatures within the range 80...293 K, are shown in Fig. 7. The absorption coefficient was calculated according to the standard method of two thicknesses [26]. Experimental absorption edge spectra show two characteristic areas, formation of which is caused by different mechanisms of light interaction with Si_2Te_3 crystalline lattice. In the long-wave part of spectra, the absorption coefficient α is weakly dependent on the photon energy, and various samples have the values within the range 30...100 cm^{-1}.

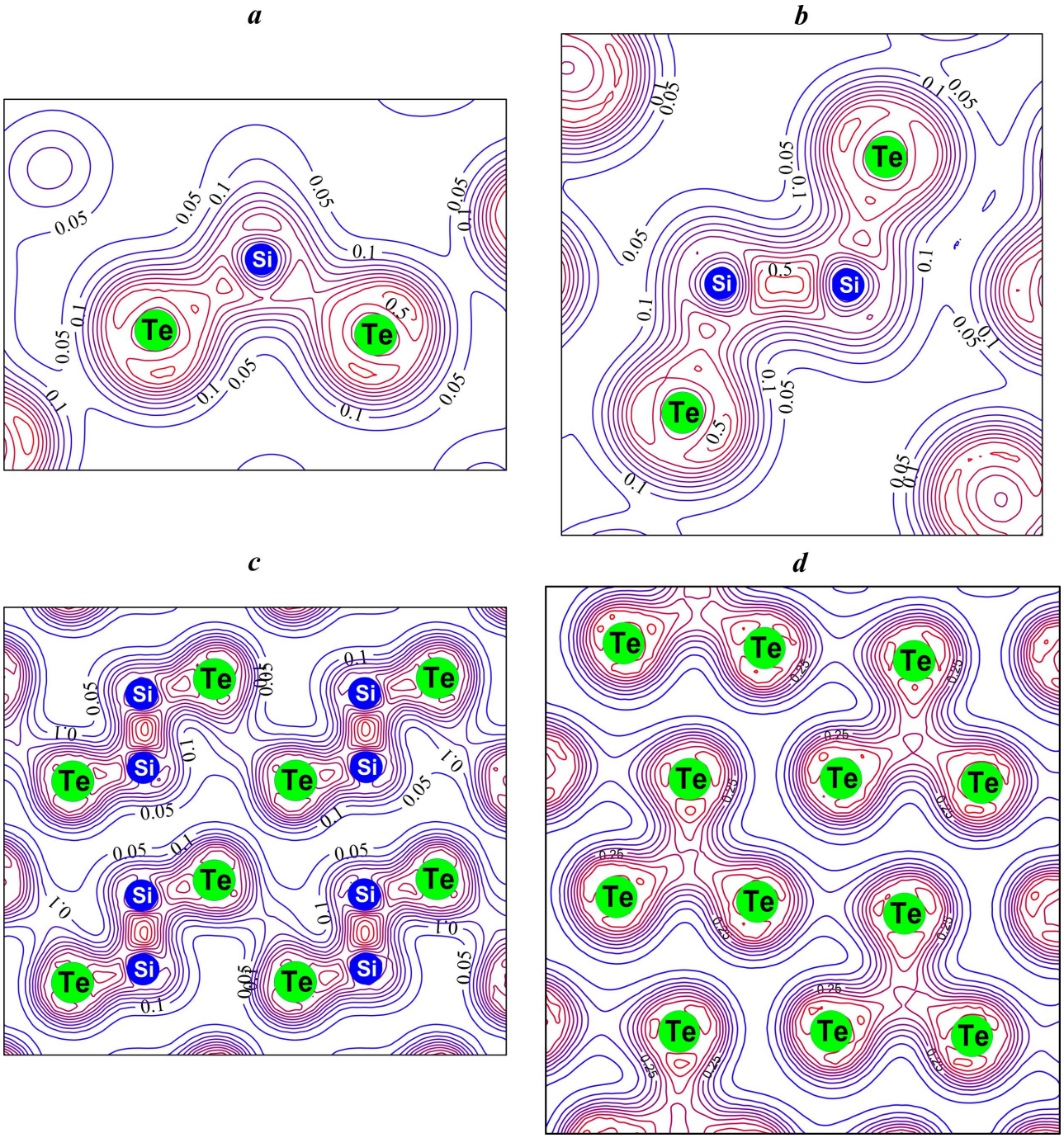

Fig. 6. Electronic density distribution maps in Si_2Te_3 crystal: (a) in the plane passing along the links lines Te–Si–Te in [$SiTe_3Si$] tetrahedron; (b) and (c) in the plane perpendicular to the four-layer packets Te–Si–Si–Te, passing through the "horizontal" (b) and "vertical" (c) dimers Si_2; (d) in the plane of the tellurium monolayer.

This long-wave part of spectra, as a rule, is associated with the presence of static defects of the lattice with different nature (uncontrolled residual impurities, pores, dislocations, cracks, *etc.*) [27, 28].

In the short-wave part of spectra (absorption coefficient takes values in the interval of $10^2...10^3$ cm^{-1}), the spectral dependence of absorption edge is described by the empirical Urbach rule [29, 30]:

$$\alpha(h\nu,T) = \alpha_0 \cdot \exp\left[\frac{\sigma(h\nu - E_0)}{kT}\right] = \alpha_0 \cdot \exp\left[\frac{h\nu - E_0}{E_U(T)}\right], \quad (1)$$

where α_0, E_0 are the coordinates of the convergence point of the Urbach "bundle"; σ is a steepness parameter of the absorption edge, $E_U = kT/\sigma$ is Urbach energy (energy width of the absorption edge), k – Boltzmann constant, T – temperature, $h\nu$ – photon energy. Fig. 7 shows that

Parameters of Urbach absorption edge and EPI for Si_2Te_3 crystal.

E_g^* (293 K) (eV)	E_U (293 K) (meV)	α_0 (cm^{-1})	E_0 (eV)	σ_0	$\hbar\omega_0$ (meV)	θ_E (K)	$(E_U)_0$ (meV)	$(E_U)_1$ (meV)	$E_g^*(0)$ (eV)	S_g^α
2.083	46.6	9.6×10^6	2.510	0.61	38.8	381	26.3	54.4	2.270	15.2

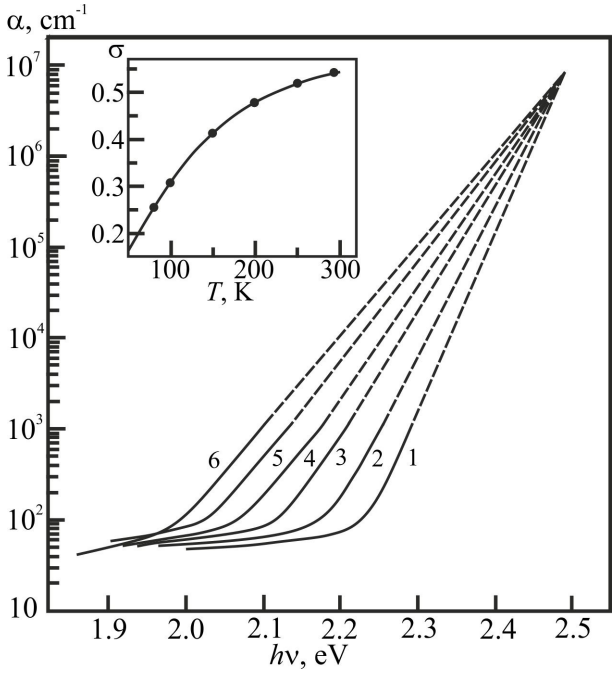

Fig. 7. Spectral dependence of the boundary absorption of the Si_2Te_3 crystal at various temperatures, K: 80 (*1*), 100 (*2*), 150 (*3*), 200 (*4*), 250 (*5*), and 293 (*6*). The insert shows the temperature dependence of the absorption edge slope.

high-energy parts of the absorption edge spectra of crystalline Si_2Te_3 within the investigated temperature range 80...293 K form the characteristic temperature "bundle" with coordinates of convergence $\alpha_0 = 9.6\cdot10^6$ cm^{-1} and $E_0 = 2.510$ eV (Table).

With increasing the temperature from 80 up to 293 K, the absorption edge is shifted to low energies (Fig. 7), which reflects a decrease in the energy band gap. The temperature dependence of absorption edge slope is described by the equation [31]:

$$\sigma(T) = \sigma_0 \cdot \left(\frac{2kT}{\hbar\omega_0}\right) \cdot \mathrm{th}\left(\frac{\hbar\omega_0}{2kT}\right), \qquad (2)$$

where σ_0 is the parameter associated with the constant of exciton(electron)-phonon interaction g by the relation $\sigma_0 = (2/3)g^{-1}$, $\hbar\omega_{ph}$ – characteristic energy of phonons that most effectively interact with electrons (excitons). For the most crystals, $\hbar\omega_{ph}$ is close to the energy of the most high-energy LO-phonon [31]. Analysis of Toyazawa criterion [32] indicates that in Si_2Te_3 crystals there is a strong electron-phonon interaction (EPI) ($\sigma_0 < 0.61 < 1$).

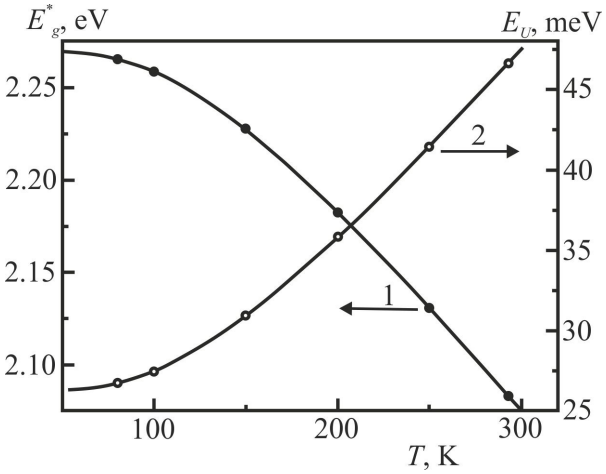

Fig. 8. Temperature dependences of the optical pseudogap E_g^* (*1*) and Urbach energy E_U (*2*) of Si_2Te_3 crystal.

The analysis of the absorption edge spectra (Fig. 7) allowed us to determine the value of the effective phonon energy (frequency) $\hbar\omega_{ph} = 38.8$ meV (313 cm^{-1}). The comparison of above mentioned value with the real values of vibrational frequencies of Si_2Te_3 crystal lattice allows to find out what type of phonons is involved into formation of the absorption edge. The obtained $\hbar\omega_{ph}$ value is close to the frequency of the longitudinal optical LO-phonon (335 cm^{-1}) which appear in the Raman spectra of Si_2Te_3 [20]. Thus, the exponential shape of Si_2Te_3 absorption edge is determined not only by the influence of charged impurities, but also by longitudinal optical LO-phonons.

Due to the fact that indirect optical transitions in Si_2Te_3 crystals are masked by long-wave Urbach absorption "tails", it is difficult to determine the true value of the energy band gap [31]. In this case, often the energy band gap is taken as the value, which corresponds to the energy position of the absorption edge at a fixed absorption level $\alpha = 10^3$ cm^{-1}. The optical pseudogap E_g^* (Fig. 8) determined in this manner is described within the Einstein model using the equation [33]:

$$E_g^*(T) = E_g^*(0) - S_g^* k\theta_E \left[\frac{1}{\exp(\theta_E/T)-1}\right], \qquad (3)$$

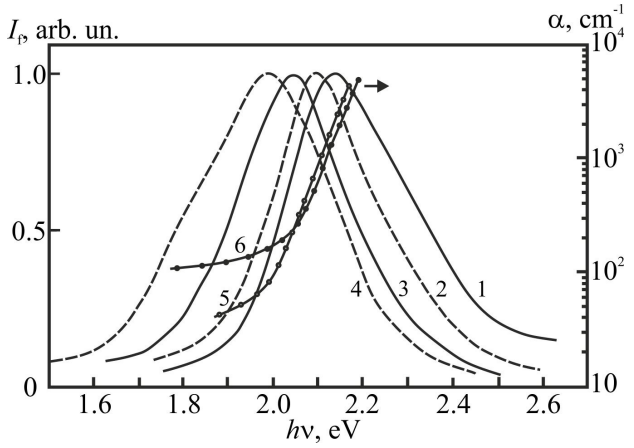

Fig. 9. Photoconductivity (*1–4*) and absorption edge (5, 6) spectra of Si_2Te_3 single crystals at various temperatures, K: 293 (*1*), 350 (*2*), 410 (*3*), and 440 (*4*) (*5* – current measurements, *6* taken from [16]).

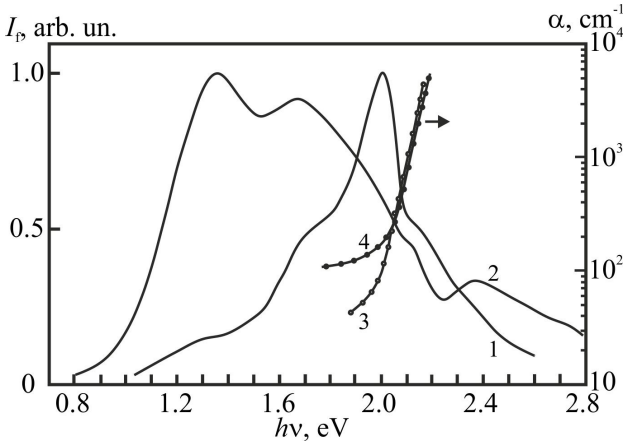

Fig. 10. Photoconductivity (*1*, *2*) and absorption edge (*3*, *4*) spectra of Si_2Te_3 single crystals at T = 293 K. (*3* – current measurements, *4* taken from [16]).

where $E_g^*(0)$ and S_g^* are, respectively, the optical pseudogap at 0 K and dimensionless constant; θ_E is the Einstein temperature that corresponds to the average frequency of phonon excitations of the system of non-interacting oscillators. $E_g^*(0)$, S_g^* and θ_E parameters obtained during the description of $E_g^*(T)$ dependence by Eq. (3) are given in Table.

Despite the fact that there is currently no single universal interpretation of the Urbach rule, there is no doubt that the exponential form of the Urbach absorption edge is caused by the influence of disordering processes. In the case of crystals, it is a dynamic (temperature) disorder, the source of which is EPI caused by lattice fluctuations, and static (structural) disorder caused by the small scale violations of the periodic potential of the crystal lattice due to the presence of point charged defects in the crystal [34–36]. The contribution of each of these factors depends on the concentration of charged impurities in material under investigation and its temperature, which determines the concentration of equilibrium phonons. With the temperature decrease, the phonons freeze, but the tails of the absorption coefficient do not disappear. Their existence is related with the heterogeneity of the crystal caused by the presence of its proper point defects. In the case of Si_2Te_3 crystals, this is primarily a high concentration of stoichiometric cationic vacancies.

The Urbach energy E_U (Fig. 8) can serve as a measure of the absorption edge smearing, and accordingly, the measure of disorder degree [37], which, as indicated above, is determined by dynamic (temperature) and static (structural) disordering [34, 38]:

$$E_U = (E_U)_X + (E_U)_T, \tag{4}$$

where $(E_U)_X$ and $(E_U)_T$ are, respectively, the contributions of structural (static) and temperature (dynamic) disordering into E_U, they are considered as independent, equivalent and additive. To separate contributions of different types of disordering into E_U, the methodology proposed by the authors was used [31]. To perform this, the known equation, well describing the temperature dependence of the Urbach energy E_U within the Einstein model, was used [34, 35]:

$$(E_U) = (E_U)_0 + (E_U)_1\left[\frac{1}{\exp(\theta_E/T)-1}\right], \tag{5}$$

where $(E_U)_0$ and $(E_U)_1$ are constant values. The values of the parameters $(E_U)_0$ and $(E_U)_1$ obtained during describing the experimental temperature dependences E_U by Eq. (4) are given in Table. Comparing the equations (4) and (5), we find the values $(E_U)_T$ = 20.3 meV (43.6% from E_U) and $(E_U)_X$ = 26.3 meV (56.4% from E_U) at T = 293 K.

3.4. Photoconductivity spectra of Si_2Te_3 crystals

Another independent method of studying the band structure is the spectral distribution of the photosensitivity of the crystal, which in general reflects the presence of two photo effects: proper and impurity ones. In the first case, there is a band-to-band bipolar generation of free carriers, in the second one, it is generation of free carriers of the same type, *i.e.*, monopolar generation related with impurity centers. Since Si_2Te_3 crystals have significant integrated photosensitivity ($\sigma_f/\sigma_t = 10^2$–10^3, where σ_f is the electrical conductivity at illumination of 10^4 lux) without special additional heat treatments, it allowed performing

studies of their photoconductivity spectra. To measure photoconductivity, gold contacts were applied to natural faces of crystalline samples, so that coplanar geometry was realized, that is, between the contacts there was a gap of 5-6 mm, through which illumination of the sample was performed.

Given that silicon sesquitelluride has a two-sided homogeneity region [39], it is important to study the influence of deviation degree of the crystal composition from stoichiometric on the spectral photosensitivity distribution. With this aim in mind, we have studied the photoconductivity spectra of Si_2Te_3 crystals grown from both stoichiometric and tellurium-surplus mixtures. Typical non-polarized photoconductivity spectra of the first type of crystals measured within the temperature range 293...440 K at a constant current and modulated illumination of the sample under study are shown in Fig. 9. As can be seen from Fig. 9, in the photoconductivity spectra of Si_2Te_3 crystals grown from the stoichiometric mixture, one wide band is observed, the energy position of the maximum of which shifts to the low-energy region with an increase of the temperature, which reflects a decrease of the energy gap value. To identify the nature of the maximum in the photoconductivity spectrum, Fig. 9 also shows the absorption edge spectra of the Si_2Te_3 crystal, measured by us (curve *5*) and taken from the Ref. [16] (curve *6*). It follows from the comparison of photoconductivity and fundamental absorption spectra that the energy position of the maximum $h\omega_{max} = 2.13$ eV in the spectrum of photoconductivity is located in the area of its proper absorption and meets value $\alpha \approx 2 \cdot 10^3$ cm^{-1}. Thus, the nature of this maximum is caused by generation of non-equilibrium carriers caused by optical band-to-band transitions (G→K) from the top of valence band formed by 5*p*-states of the tellurium lone pair to the bottom of the conductivity band formed by kneading of free *p*-states of tellurium and silicon (Figs. 4 and 5).

This naturally raises the question, what is the exact way to determine the value of the energy gap from the photoconductivity spectra of the Si_2Te_3 crystal? In the study of homopolar semiconductor (Si, Ge, *etc*.) photoconductivity, the fundamental absorption edge is sharply pronounced, and E_g is determined beyond the threshold of photoconductivity (Moss rule). However, in the case of Si_2Te_3 crystals, the frequency dependence of the absorption coefficient $\alpha(\omega)$ in the region of fundamental absorption edge at $\alpha \leq 10^3$ cm^{-3} (Fig. 7) is not a root one, as in the case of direct optical transitions in ideal semiconductors. In this case, as shown in Ref. [40], in wide-band crystals with the exponential dependence of the long-wave absorption edge in wide range of the thickness of samples and velocities of surface recombination, the effective value of energy gap can be determined with great accuracy by the effective position of the intrinsic maximum in the spectrum of photoconductivity. Thus, if the energy of interband transitions is estimated by the spectral position of the intrinsic maximum of photoconductivity, then it follows from the photoconductivity spectra given in Fig. 9 that the energy gap value of Si_2Te_3 crystal equals $E_g = 2.13$ eV at room temperature.

It should be noted that even when Si_2Te_3 crystals are grown from a stoichiometric mixture, in the same ampoule, the crystals grow with a different from the above-described photoconductivity spectrum (curve *1*, Fig. 10). As can be seen from Fig. 10, the photosensitivity of these crystals manifests itself in a wider spectral range of 1.0…2.5 eV, and the photoconductivity spectrum is complex and contains a pronounced intense peak at 2.02 eV, one feature in the form of an influx at 2.12 eV at a high energy downturn of the main peak and two features at 1.7 and 1.32 eV at a long-wave downturn.

The authors of Refs [17, 18] give close in their form photoconductivity spectra of Si_2Te_3 crystals, in which at $T = 93$ K there is an intense band with a maximum at 2.2 eV in the range of fundamental absorption, a feature in the form of an inflection at 1.9 eV on the long-wave decline of the main band and a wide long-wave band with the maximum close to 1 eV.

The photoconductivity spectrum of non-stoichiometric Si_2Te_3 crystals, grown from the original mixture containing the excess of tellurium, is undergoing even greater changes (curve *2*, Fig. 10). It can be seen from Fig. 10 that impurity bands with the maxima at 1.65 and 1.33 eV are dominant in the photoconductivity spectrum, while the intensity of its intrinsic maximum sharply decreases, and it manifests itself in the form of inflection at ~2.1 eV. Given that non-stoichiometric Si_2Te_3 crystals contain both silicon vacancies (by the nature of the substance itself) and excess tellurium atoms, additional complex studies of stationary and kinetic characteristics of photoconductivity are necessary to establish the nature of impurity bands in the photoconductivity spectra.

4. Conclusions

Calculations of the electronic structure, the total and partial densities of states, and the spatial distribution of the electron charge density of a Si_2Te_3 crystal are performed for an optimized structure by using *ab initio* the density functional theory method in the LDA+*U* approximation. The calculation and analysis of the total and partial densities of the electron states of the $N(E)$ silicon sesquitelluride made it possible to determine the genesis of the individual subbands and their band structure as a whole.

It is shown that the dependence of the absorption coefficient on the photon energy is described by the Urbach rule. An estimation of the contribution of structural and dynamic disorder to the smearing of the absorption edge of a Si_2Te_3 crystal has been performed. The parameters of the Urbach absorption edge and the electron-phonon interaction have been determined.

The effect of deviation of the composition from the stoichiometric one on the photoconductivity spectra of layered Si_2Te_3 crystals has been studied.

References

1. Ploog K., Stetter W., Nowitzki A., Schönherr E. Crystal growth and structure detrmination of silicon telluride Si_2Te_3. *Mater. Res. Bull*. 1976. **11**, No 8. P. 1147–1154. https://doi.org/10.1016/0025-5408(76)90014-3.
2. Gregoriades P.E., Bleris G.L., Stoemenos J. Electron diffraction study of the Si_2Te_3 structural transformation. *Acta Crystallogr. B*. 1983. **39**. P. 421–426. https://doi.org/10.1107/S0108768183002670.
3. Parsonage N.G., Staveley L.A.K. *Disorder in Crystals*. Clarendon Press, Oxford, 1978.
4. Keuleyan S., Wang M., Chung F.R., Commons J., Koski K.J. A silicon-based two-dimensional chalcogenide: Growth of Si_2Te_3 nanoribbons and nanoplates. *Nano Lett*. 2015. **15**. P. 2285–2290. https://doi.org/10.1021/nl504330g.
5. Juneja R., Pandey T., Singh A.K. High thermoelectric performance in *n*-doped silicon-based chalcogenide Si_2Te_3. *Chem. Mater*. 2017. **29**. P. 3723–3730. https://doi.org/10.1021/acs.chemmater.7b00728.
6. Wu K., Sun W., Jiang Y., Chen J., Li L., Cao C., Shi S., Shen X., Cui J. Structure and photoluminescence study of silicon based two-dimensional Si_2Te_3 nanostructures. *J. Appl. Phys*. 2017. **122**. P. 075701-1–075701-8. https://doi.org/10.1063/1.4998811.
7. Wang M., Lahti G., Williams D., Koski K.J. Chemically tunable full spectrum optical properties of 2D silicon telluride nanoplates. *ACS Nano*. 2018. **12**. P. 6163–6169. https://doi.org/10.1021/acsnano.8b02789.
8. Wu K., Cui J. Morphology control of Si_2Te_3 nanostructures synthesized by CVD. *J. Mater. Sci. Mater. Electron*. 2018. **29**. P. 15643–15648. https://doi.org/10.1007/s10854-018-9158-1.
9. Wu K., Chen J., Shen X., Cui J. Resistive switching in Si_2Te_3 nanowires. *AIP Adv*. 2018. **8**. P. 125008-1–125008-7. https://doi.org/10.1063/1.5060675.
10. Chen J., Wu K., Shen X., Hoang T.B., Cui J. Probing the dynamics of photoexcited carriers in Si_2Te_3 nanowires. *J. Appl. Phys*. 2019. **125**. P. 024306-1–024306-1. https://doi.org/10.1063/1.5053932.
11. Roberts G.G., Lind E.L. Space charge conduction in single crystal Si_2Te_3. *Phys. Lett. A*. 1970. **33**. P. 365–366. https://doi.org/10.1016/0375-9601(70)90833-9.
12. Ziegler K., Junker H.-D., Birkholz U. Electrical conductivity and Seebeck coefficient of Si_2Te_3 single crystals. *phys. status solidi (a)*. 1976. **37**. P. K97–K99. https://doi.org/10.1002/pssa.2210370166.
13. Bauer H.P., Birkholz U. Electrical conductivity of passivated Si_2Te_3 single crystals. *phys. status solidi (a)*. 1978. **49**. P. 127–131. https://doi.org/10.1002/pssa.2210490114.
14. Rick M., Rosenzweig J., Birkholz U. Anisotropy of electrical conductivity in Si_2Te_3. *phys. status solidi (a)*. 1984. **83**. P. K183–K186. https://doi.org/10.1002/pssa.2210830260.
15. Vennik J., Callaerts R. Sur les proprietes optiques du tellurure de silicium Si_2Te_3. *C.R. Acad. Sci. Paris*. 1965. **260**. P. 496–499.
16. Bruckel B., Birkholz U., Ziegler K. Fundamental absorption and Franz–Keldysh effect in silicon telluride. *phys. status solidi (a)*. 1976. **78**. P. K23–K25. https://doi.org/10.1002/pssb.2220780147.
17. Ziegler K., Berkholz P. Photoconductivity of Si_2Te_3 single crystals. *phys. status solidi (a)*. 1976. **37**. P. K147–K149. https://doi.org/10.1002/pssa.2210370254.
18. Ziegler K., Berkholz P. Photoelectric properties of Si_2Te_3 single crystals. *phys. status solidi (a)*. 1977. **39**. P. 467–475. https://doi.org/10.1002/pssa.2210390213.
19. Petersen K.E., Birkholz U., Adler D. Properties of crystalline and amorphous silicon telluride. *Phys. Rev. B*. 1973. **8**. P. 1453–1461. https://doi.org/10.1103/PhysRevB.8.1453.
20. Zwick U., Rieder K.H. Infrared and Raman study of Si_2Te_3. *Z. Physik B*. 1976. **25**. P. 319–322. https://doi.org/10.1007/BF01315246.
21. Vakulchak V.V. Electronic structure of silicon and germanium dichalcogenides and $M_2Si(Ge)S_3$ (M = = Li, Na, Ag) superionics: The dissertation for the degree of a doctor of philosophy, Uzhhorod, 2015 (in Ukrainian).
22. Shen X., Puzyrev Y.S., Combs C., Pantelides S.T. Variability of structural and electronic properties of bulk and monolayer Si_2Te_3. *Appl. Phys. Lett.* 2016. **109**. P. 113104-1–113104-5. https://doi.org/10.1063/1.4962826.
23. Anisimov V.I., Aryasetiawan F., Lichtenstein A.I. First-principles calculations of the electronic structure and spectra of strongly correlated systems: the LDA+U method. *J. Phys.: Condens. Matter*. 1997. **9**. P. 767–808. https://doi.org/10.1088/0953-8984/9/4/002.
24. SIESTA is both a method and its computer program implementation, to perform efficient electronic structure calculations and *ab initio* molecular dynamics simulations of molecules and solids / http://icmab.cat/leem/siesta/.
25. Bletskan D.I., Glukhov K.E., Frolova V.V. Electronic structure of 2*H*-$SnSe_2$: *ab initio* modeling and comparison with experiment. *Semiconductor Physics Quantum Electronics & Optoelectronics.* 2016. **19**. P. 98–108.
26. Ukhanov Yu.I. *Optical Properties of Semiconductors.* Moscow: Nauka, 1977 (in Russian).
27. Tsebulya G.G., Lisitsa M.P., Malynko V.N. New interpretation of red absorption of Ge and CdTe. *Ukr. Fiz. Zhurnal.* 1967. **12**. P. 1144–1150 (in Russian).

28. Froza A., Selloni A. *Tetragedrally-bonded Amorphous Semiconductors.* N.Y.: London, 1985.
29. Urbach F. The long-wavelenth edge of photographic sensitivity and of the electronic absorption of solids. *Phys. Rev*. 1953. **92**. P. 1324–1331. https://doi.org/10.1103/PhysRev.92.1324.
30. Toyozawa Y. Theory of line-shapes of the exciton absorption bands. *Progress of Theoretical Physics*. 1958. **20**. P. 53–81. https://doi.org/10.1143/PTP.20.53.
31. Studenyak I.P., Kranjčec M., Kurik M.V. *Optics of Disordered System*. Uzhhorod: Grazhda, 2008 (in Ukrainian).
32. Sumi H., Toyozawa Y. Urbach–Martiensen rule and exciton trapped momentaliry by lattice vibration. *J. Phys. Soc. Jpn*. 1971. **31**, No 2. P. 342–358. https://doi.org/10.1143/JPSJ.31.342.
33. Beaudoin M., DeVries A.J.G., Johnson S.R., Laman H., Tiedje T. Optical absorption edge of semi-insulating GaAs and InP at high temperatures. *Appl. Phys. Lett.* 1997. **70**. P. 3540–3542. https://doi.org/10.1063/1.119226.
34. Cody G.D., Tiedje T., Abeles B., Brooks B., Goldstein Y. Disorder and the optical-absorption edge of hydrogenated amorphous silicon. *Phys. Rev. Lett*. 1981. **47**. P. 1480–1483. https://doi.org/10.1103/PhysRevLett.47.1480.
35. Johnson S.R., Tiedje T. Temperature dependence of the Urbach edge in GaAs. *J. Appl. Phys*. 1995. **78**. P. 5609–5613. https://doi.org/10.1063/1.359683.
36. Sa-Yakanit V., Glyde H.R. Urbach tails and disorder. *Comments Matter Phys.* 1987. **13**, No 1. P. 35–48.
37. Pistoulet B., Robert J.L., Dusseau J.M., Ensuque L. Conduction mechanisms in amorphous and disordered semiconductors explained by a model of medium-range disorder of composition. *J. Non-Crystal. Solids*. 1978. **29**. P. 29–40. https://doi.org/10.1016/0022-3093(78)90137-0.
38. Tauc J. Absorption edge and internal electric fields in amorphous semiconductors. *Mater. Res. Bull*. 1970. **5**. P. 721–729. https://doi.org/10.1016/0025-5408(70)90112-1.
39. Odin I.N., Ivanov V.A. State P_{tot}–T–x-diagram of Si–Te system. *Zhurnal Neorg. Khimii.* 1991. **36**. P. 1314–1319 (in Russian).
40. Vlasenko A.I., Vlasenko Z.K., Lyubchenko A.V. Photoconductivity spectral characteristics of semiconductors with exponential fundamental absorption edge. *Semiconductors*. 1999. **33**, Issue 11. P. 1171–1174.

Authors and CV

Dmytro I. Bletskan, born in 1946, defended his Doctoral Dissertation in Physics and Mathematics in 1985 and became full professor in 1988. Professor of the Department physics of semiconductors at the Uzhhorod National University, Ukraine. Authored over 260 scientific publications, 86 patents, 2 textbooks, 2 monographs. The area of his scientific interests – technology and physics of highly anisotropic layered crystals, physical properties of chalcogenide glassy semiconductors and superionics.

Vasyl V. Vakulchak, born in 1986, defended his PhD thesis in Physics and Mathematics in 2015. Senior researcher of the Department of Applied Physics at the Uzhhorod National University, Ukraine. Authored of 60 scientific publications and 1 patent. The area of scientific interests is *ab initio* calculation of the electronic structure, physical properties of semiconductors.

Ihor P. Studenyak, born in 1960, defended his Dr. Sc. degree in Physics and Mathematics in 2003 and became full professor in 2004. Vice-rector for research at the Uzhhorod National University, Ukraine. Authored over 200 publications, 120 patents, 15 textbooks. The area of his scientific interests includes physical properties of semiconductors, ferroics and superionic conductors.